Journal of Luminescence 155 (2014) 170–179

Contents lists available at ScienceDirect

Journal of Luminescence

journal homepage: www.elsevier.com/locate/jlumin

Influence of Ge content and annealing conditions on the PL properties of nc-$Si_{1-x}Ge_x$ embedded in SiO_2 matrix in weak quantum confined regime

Evrin Tuğay [a,*], Serim Ilday [b,c], Raşit Turan [c,d], Treje G. Finstad [e]

[a] Department of Mechanical Engineering, Faculty of Engineering, Recep Tayyip Erdogan University, Rize 53100, Turkey
[b] Department of Micro & Nanotechnology, Middle East Technical University, Ankara, Turkey
[c] Center of Solar Energy Research and Application (GÜNAM), Middle East Technical University (METU), 06531 Ankara, Turkey
[d] Department of Physics, Middle East Technical University, Ankara, Turkey
[e] Department of Physics, University of Oslo, Oslo, Norway

ARTICLE INFO

Article history:
Received 25 April 2013
Received in revised form
24 December 2013
Accepted 9 June 2014
Available online 26 June 2014

Keywords:
$Si_{1-x}Ge_x$ nanocrystals
Photoluminescence
Quantum confinement
Defects

ABSTRACT

Fabrication of Si (nc-Si), Ge (nc-Ge), and $Si_{1-x}Ge_x$ (nc-$Si_{1-x}Ge_x$) nanocrystals embedded in SiO_2 matrix is achieved by thermal annealing of magnetron-sputtered thin films. Effects of annealing conditions, namely duration and temperature, as well as Ge content on the photoluminescence properties are investigated. Origin and evolution of the photoluminescence signal in the weak quantum confinement regime are discussed. It is found that photoluminescence signals can be decomposed into four Gaussian peaks originating from Ge-related radiative defects located at the sub-oxide (GeO_x), either inside the matrix or at the interface region (peak M), nc-$Si_{1-x}Ge_x$/SiO_2 interface-related localized states (peak I), localized states in the amorphous $Si_{1-x}Ge_x$ bandgap (peak A) and quantum confinement of excitons in small nanocrystals (peak Q). The role of small and large nanocrystals in the photoluminescence mechanism is investigated by varying the mean nanocrystal size from 3 nm to 23 nm (from strong to weak quantum confined regime). Our results demonstrate that the quantum confinement effect in Ge nanocrystals manifests though spectral blueshift due to increase in Ge content. We also propose that the decreasing photoluminescence signal intensity with an increase in Ge content may originate from Ge-related nonradiative P_b centers.

© 2014 Elsevier B.V. All rights reserved.

1. Introduction

Rapidly growing interest in using silicon (nc-Si) and germanium nanocrystals (nc-Ge) in optoelectronic devices drives attention to their optical properties, particularly to the origin of the photoluminescence (PL) emission from these nanocrystals and the underlying mechanism. Much of this activity has been focused on the identification of nc-Si PL mechanism and it is known that the decrease in nc-Si size leads to a spectral blueshift accompanied by an increase in the PL signal intensity. On the other hand, compared to their nc-Si counterparts, studies on the size-dependent PL emission of nc-Ge are still in the early stages [1–7]. Furthermore, while most of the research on PL mechanism of the nc-Si and nc-Ge agree on the important role of quantum confinement of excitons, it is clear that other mechanisms also play a role [8–14]. We note that, since 1992, more than 20 mechanisms have been proposed to underlie PL emission from these nanocrystals [15]. In short, the subject needs further investigation and insight.

An alternative and promising approach to investigate the PL mechanism of nc-Si and nc-Ge is to study nanocrsytals of $Si_{1-x}Ge_x$ (nc-$Si_{1-x}Ge_x$) alloys, where one can observe and study the continuum of PL signal evolution from Si-rich to Ge-rich region. Although there are several reports on the PL emission of nc-$Si_{1-x}Ge_x$/SiO_2 system and its mechanism [16–21], conclusive results have not been obtained.

Here, we report an extensive PL analysis of the magnetron sputtered thin films composed of nc-Si, nc-Ge, and nc-$Si_{1-x}Ge_x$ embedded in SiO_2 matrix, where the nanocrystal sizes range between the exciton Bohr radius of Si (~5 nm) and that of Ge (~24 nm). In order to fully investigate and understand the PL mechanism and the role of small and large nanocrystals, PL signal evolution from Si-rich to Ge-rich region is scrutinized by carefully tailoring the Ge content of the thin films. The PL emission between 1.24eV and 2.22 eV is decomposed into four Gaussian peaks and analyzed. The PL spectra is identified in terms of Ge-related radiative defects located at the sub-oxide (GeO_x), either inside

* Corresponding author.
E-mail address: evrin.tugay@erdogan.edu.tr (E. Tuğay).

http://dx.doi.org/10.1016/j.jlumin.2014.06.012
0022-2313/© 2014 Elsevier B.V. All rights reserved.

the matrix or at the interface region (peak M), nc-$Si_{1-x}Ge_x/SiO_2$ interface-related localized states (peak I), localized states in the amorphous $Si_{1-x}Ge_x$ bandgap (peak A) and quantum confinement of excitons in small nanocrystals (peak Q). We clearly demonstrate that the quantum confinement effect in nc-Ge is manifested by a spectral blueshift and we further show that Ge content plays an important role as well as the annealing conditions in the PL mechanism of nc-$Si_{1-x}Ge_x/SiO_2$ system.

2. Experimental details

SiO_2/SiO_2:Si:Ge/SiO_2 sandwich thin films are deposited onto Si (1 0 0) substrate using magnetron-sputtering. 3 in.-diameter SiO_2, Si, and Ge targets are co-sputtered with RF (P_{SiO2}=350 W) and DC powers applied (P_{Si}=0 and 100 W, and P_{Ge}=0, 7, 10, and 20 W), respectively. In order to study the effect of Ge content on the PL spectra, we have varied the DC power applied to the Ge target, while keeping DC and RF powers applied to the Si and SiO_2 targets fixed. Bottom and topmost SiO_2 layers with 40 nm thicknesses are used to restrain the formation of poly-Ge and/or SiGe precipitates or the intermixing of Si and Ge at the substrate/thin film interface during post-annealing. The thickness of the co-sputtered layer is fixed at 250 nm in all experiments and the deposition rate is kept at 4 nm/min. Post-annealing studies are carried under flowing N_2 atmosphere in a high-temperature furnace. Samples have been annealed at three different temperatures (T) namely 900, 1000, and 1100 °C and the annealing time (t) has been varied between 1 and 5 h.

First, the formation and evolution of nc-Si, nc-Ge, and nc-$Si_{1-x}Ge_x$ are characterized through high-resolution cross-sectional transmission electron microscope (HRTEM) [JEOL2010F]. Next, the crystal structure is determined from X-ray diffraction spectroscopy (XRD) [Rigaku Miniflex System with Cu K_α line]. PL measurements were made at room temperature using the second harmonic (532 nm) of a Nd:YAG laser. For the PL peak fitting analyses the least square fitting method to the Levenberg–Marquardt (L–M) algorithm using Origin software is applied. Finally, chemical bond characteristics and atomic percentages of the existing species in the system were determined through Raman (RS) [HR800, Jobin Yvon using a He–Ne laser at 632.8 nm], and Fourier-transform infrared spectroscopies (FTIR) [Bruker Equinox spectrometer] analyses.

3. Results and discussion

3.1. nc-$Si_{1-x}Ge_x$ formation and its structural properties

Formation of the nanocrystals is verified by HRTEM, XRD, and RS measurements. Fig. 1(a–d) shows the cross-sectional HRTEM images and corresponding selected area diffraction (SAD) patterns of the SiO_2/Si:Ge:SiO_2/SiO_2 thin films for which the growth and annealing conditions were P_{Ge}=20 W, T=900 °C, t=1 h for Fig. 1a, P_{Ge}=20 W, T=1100 °C, t=1 h for Fig. 1b, P_{Ge}=20 W, T=1100 °C, t=3 h for Fig. 1c and P_{Ge}=7 W, T=1100 °C, t=1 h for Fig. 1d, respectively. As can be seen from Fig. 1a, small nanocrystals with average sizes of 5 nm are just starting to form following the post-annealing procedure at 900 °C for 1 h and the corresponding SAD pattern suggests that the structure is mostly amorphous. Increasing the annealing temperature to 1100 °C (Fig. 1b) leads to the formation of larger nanocrystals with average sizes of 23 nm within which the crystallinity is further improved (evidenced by discrete spots of the SAD pattern). As we have demonstrated in a recent study [22], prolonged annealing times at high temperatures (at 1100 °C) does not affect the average nanocrystal size, but it leads to the formation of nanostructures where Si-rich SiGe core is covered by a Ge-rich SiGe shell. Similarly, in this study we observe a core–shell structure as well, which can be seen through Fig. 1c. It is observed that if the P_{Ge} is decreased from 20 W to 7 W, the average nanocrystal size is also decreases from 23 to 9 nm when the post-annealing conditions are kept constant (T=1100 °C, t=1 h) (Fig. 1d).

XRD spectra of the fabricated nc-$Si_{1-x}Ge_x$ alloys along with Si (1 1 1) and Ge (1 1 1) diffraction peaks are presented in Fig. 2. Fig. 2a shows the effect of annealing conditions on the SiO_2/Si:Ge:SiO_2/SiO_2 thin films prepared at P_{Ge}=20 W, whereas Fig. 2b shows the effect of Ge content on the SiO_2/Si:Ge:SiO_2/SiO_2 thin films, annealed at 1100 °C for 1 h. As expected, Fig. 2a shows the amorphous nature of the as-deposited sample, the sample to which no post-annealing treatment is applied, and the appearance of the (1 1 1) diffraction peak between Si (1 1 1) and Ge (1 1 1) Bragg peaks in post-annealed samples is indication of crystallized structure. It is also seen that the increasing the annealing temperature from 900 to 1100 °C leads to an increase in the average sizes of nc-$Si_{1-x}Ge_x$ and in improved crystallinity as evidenced by the increased XRD signal intensity and reduced full-width at half-maximum (FWHM) of the peak. With prolonged annealing times at 1100 °C, the intensity of the peak centered at around 27.85° decreases and decomposes into two distinct Gaussian peaks centered at around 27.65° and 27.85°, respectively. We attribute this to the formation of a core–shell structure in Ge-rich nc-$Si_{1-x}Ge_x$ as shown in Fig. 1c and discussed in our previous study [22]. Furthermore, Fig. 2b shows pure Si (1 1 1) and pure Ge (1 1 1) crystal diffraction peaks as well as the evolution of XRD spectra from Si-rich to Ge-rich region, where the spectral shift from pure Si (1 1 1) towards pure Ge (1 1 1) peak is observed when Ge content is increased. We have calculated the amount of Ge content "x" from XRD analyses using the relationship between lattice constant and Ge content, assuming that $Si_{1-x}Ge_x$ alloy system is relaxed [23]. We have to stress that the x values are not absolute since there is possibility of stress development on the nanocrystals. For the samples annealed at 1100 °C for 1 h and prepared using P_{Ge}=7, 10, and 20 W, we obtain x values to be 0.41, 0.45, and 0.69, respectively.

We have conducted RS analyses in order to monitor the evolution of nc-$Si_{1-x}Ge_x$ PL emission (Fig. 3). In general, Raman spectra of the nc-$Si_{1-x}Ge_x$ alloy consist of three main peaks due to the nearest-neighbor Ge–Ge (~300 cm^{-1}), Si–Ge (~400 cm^{-1}), and Si–Si (~500 cm^{-1}) stretching vibrations [24]. The signal originating from Si–Si stretching vibrations is weak in Ge-rich nc-$Si_{1-x}Ge_x$ and is partially masked by the intense signal originating from the Si substrate. As can be seen from Fig. 3, an increase in the annealing temperature affects both the Ge–Ge and Ge–Si vibrations; not only peak intensities increase but also Ge–Si peak shifts towards the Ge–Ge peak, towards lower frequencies. Evolution of the Ge–Ge peak as well as the Ge–Si peak as a result of the increased annealing temperature is consistent with improved crystallinity, which is evidenced by Fig. 2b where FWHM of the signal decreases and its intensity increases. The Si–Si longitudinal optical (LO) peak, originating from the Si substrate (evidenced around 301 cm^{-1}) is suppressed by the intense Ge–Ge peak for the sample annealed at 1100 °C. There is also a broad amorphous component observed in RS spectra that is centered at ~270 cm^{-1} for all annealing temperatures, confirming the remaining presence of amorphous features, which is more prominent for the sample annealed at 900 °C.

3.2. Influence of Ge content and annealing conditions on nc-$Si_{1-x}Ge_x$ PL emission

3.2.1. Influence of the annealing conditions on nc-Si (P_{Ge}=0 W) PL emission

The dependence of the PL spectra on the annealing conditions (temperature and time) of the sample that has no Ge content (P_{Ge}=0 W) is shown in Fig. 4. Fig. 4(b–g) shows peak fitting analyses, where the left column represents the effect of annealing

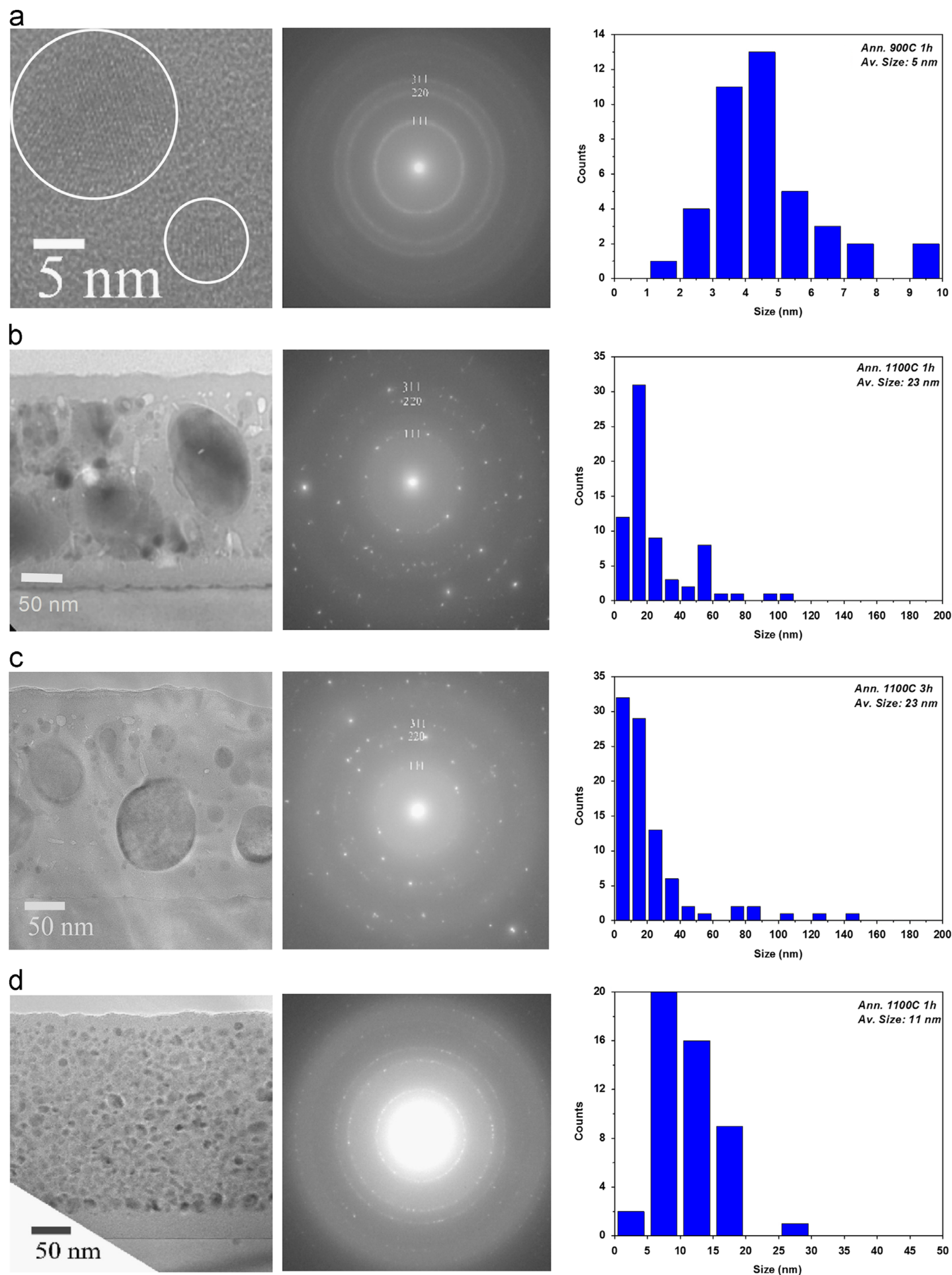

Fig. 1. Cross-sectional HRTEM images and corresponding SAD patterns of the SiO_2/Si:Ge:SiO_2/SiO_2 thin films of which the growth and annealing conditions are (a) P_{Ge}=20 W, T=900 °C, t=1 h, (b) P_{Ge}=20 W, T=1100 °C, t=1 h, (c) P_{Ge}=20 W, T=1100 °C, t=3 h, and (d) P_{Ge}=7 W, T=1100 °C, t=1 h.

temperature and the right column represents the effect of annealing time. As can be seen from the figure, all samples exhibit a broad PL emission between 480 nm and 1050 nm at room temperature. This phenomenon is often associated with a broad size distribution of nanocrystals inside the matrix [25,26]. The spectra show a peak centered at around 600 nm for the as-deposited sample. When annealed at 900 °C for 1 h, the spectra shifts to higher frequencies due to precipitation of the nanocrystals. Further increase in the annealing temperature leads to the formation of a well-defined interface between the nanocrystals and the surrounding matrix. This also leads to increased crystallinity and larger average nanocrystal sizes. In addition, the spectra shifts towards higher frequencies when annealing time is increased at 1100 °C.

In order to understand the underlying mechanism of PL emission, we have decomposed this broad peak into four Gaussian peaks (Fig. 4(b–f)), which we have labeled and attributed to:

- peak M (610–626 nm): Ge-related radiative defects located at the sub-oxide (GeO_x), either inside the matrix or at the interface region [27,28],
- peak Q (780–801 nm): quantum confinement of excitons in small nanocrystals [1,7,28–30],

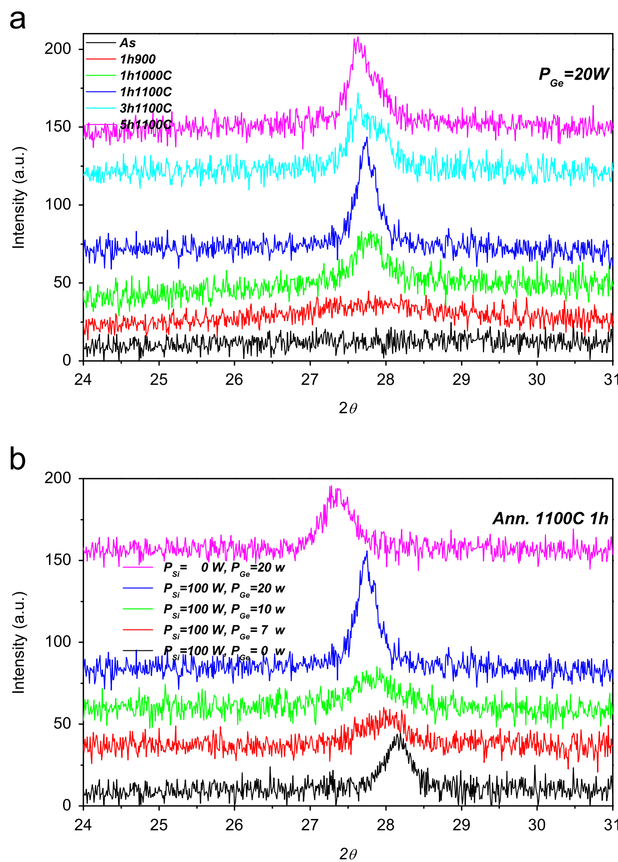

Fig. 2. XRD spectra showing (a) the effect of annealing conditions on the SiO_2/Si:Ge:SiO_2/SiO_2 thin films that are prepared using $P_{Ge}=20$ W and (b) the effect of Ge content on the SiO_2/Si:Ge:SiO_2/SiO_2 thin films that are annealed at $T=1100$ °C for $t=1$ h.

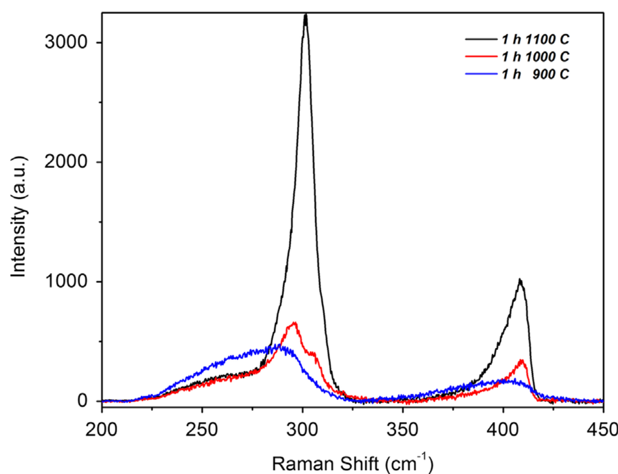

Fig. 3. Raman spectra showing the effect of annealing temperature on the SiO_2/Si:Ge:SiO_2/SiO_2 thin films that are prepared using $P_{Ge}=20$ W.

- peak I (894–914 nm): nc-$Si_{1-x}Ge_x$/SiO_2 interface-related localized states [26,28], and
- peak A (984–1000 nm): localized states in the amorphous $Si_{1-x}Ge_x$ bandgap.

Peak M is generally attributed to the radiative defects in SiO_2 matrix [27,28]. A PL signal in this range (~600–630 nm) has also been observed in nc-Si/SiO_2 systems, which is understood to be originating from the non-bridging oxygen hole centers (NBOHC) located inside the SiO_2 matrix [27,28]. However, the intensity of the peak M is increased significantly accompanied by spectral shift with Ge incorporation, which suggests that the signal is originating from the Ge-related radiative defects located at the sub-oxide (GeO_x), either inside the matrix or at the interface region [27,28].

In our previous report [28], we have discussed the evolution of the four-abovementioned recombination mechanisms with respect to the annealing conditions (temperature and time) for nc-Si in detail by conducting temperature-dependent PL measurements (emission energy and integrated intensity). We have concluded that the crystallinity, size, radiative centers, nonradiative defects, and the energy transfer between the nanocrystals also contribute to the PL emission from nc-Si. In Fig. 4, we show the PL emission of the sample devoid of Ge as a reference on the effect of Ge content "x" on the PL emission from nc-$Si_{1-x}Ge_x$.

3.2.2. Influence of annealing conditions on nc-$Si_{1-x}Ge_x$ ($P_{Ge}=10$ W) PL emission

Fig. 5 shows the evolution of the PL spectra with respect to the annealing conditions of the SiO_2/Si:Ge:SiO_2/SiO_2 thin films that were prepared using $P_{Ge}=10$ W with the experimental conditions kept identical to that of the Ge-devoid ($P_{Ge}=0$ W) test samples as control experiment. Compared to Fig. 4, the most striking feature in Fig. 5 is the abrupt decrease in PL intensity (by about two orders of magnitude) with incorporation of Ge to the system. We relate this decrease to increased density of defects when Ge is introduced, as these defects act as nonradiative recombination centers. Schoisswohl et al. [31] have reported an electron spin resonance (ESR) study on the density of defects for oxidized porous $Si_{0.8}Ge_{0.2}$ and they found out that the density of Ge P_b centers is significantly larger than that of Si P_b centers. In another ESR study on nc-$Si_{1-x}Ge_x$ Toshikiyo et al. [32] found out that the obtained ESR spectrum is a superposition of the signals originating from Si and Ge P_b centers. In their study, Toshikiyo et al. [32] have shown that the signal originating from Ge P_b centers is increased with increasing Ge concentration, while the signal originating from Si P_b centers is nearly independent of Ge concentration. Ge P_b centers have defect levels in the nc-$Si_{1-x}Ge_x$ bandgap, which are deeper in energy than those of Si P_b centers. They have demonstrated a clear correlation between increasing number of Ge P_b centers and decreasing PL signal intensity, as we have also observed and confirmed experimentally.

Another prominent feature of the Fig. 5 is the broad PL spectra observed between 480nm and 1050 nm where the most intense PL signal is observed for 1100 °C annealed samples for prolonged annealing durations of 3 and 5 h. In order to investigate the origin and evolution of the PL emission with respect to the annealing conditions and to distinguish the role of quantum confinement effect and interface-related radiative defects, we have decomposed the PL spectra into four Gaussian peaks as shown in Fig. 5(b–g). Fig. 5(b–d) shows the effect of annealing temperature, whereas Fig. 5(e–g) shows the effect of annealing time to the PL emission, respectively. Before commenting on Fig. 5, it is necessary to first discuss the structural damage on the SiO_2 network fabricated by co-sputtering and its repair by the post-annealing treatment. This will help determine the relationship between the radiative defect characteristics and the observed PL spectra. To this end, we have resorted to FTIR analysis.

Fig. 6a shows the FTIR absorption spectra of the as-deposited SiO_2 and co-sputtered SiO_2/Si:Ge:SiO_2/SiO_2 thin films, which were prepared at $P_{Ge}=10$ W. The well-known symmetric stretching (SS, ~810 cm^{-1}) and asymmetric stretching (AS, ~1084 cm^{-1}) absorption modes of the Si–O–Si bridging bond [33] are shown in the figure. A detailed discussion on the identification of different absorption modes via FTIR analyses and their significance to nanocrystal formation is discussed in Ref. [34], where we have

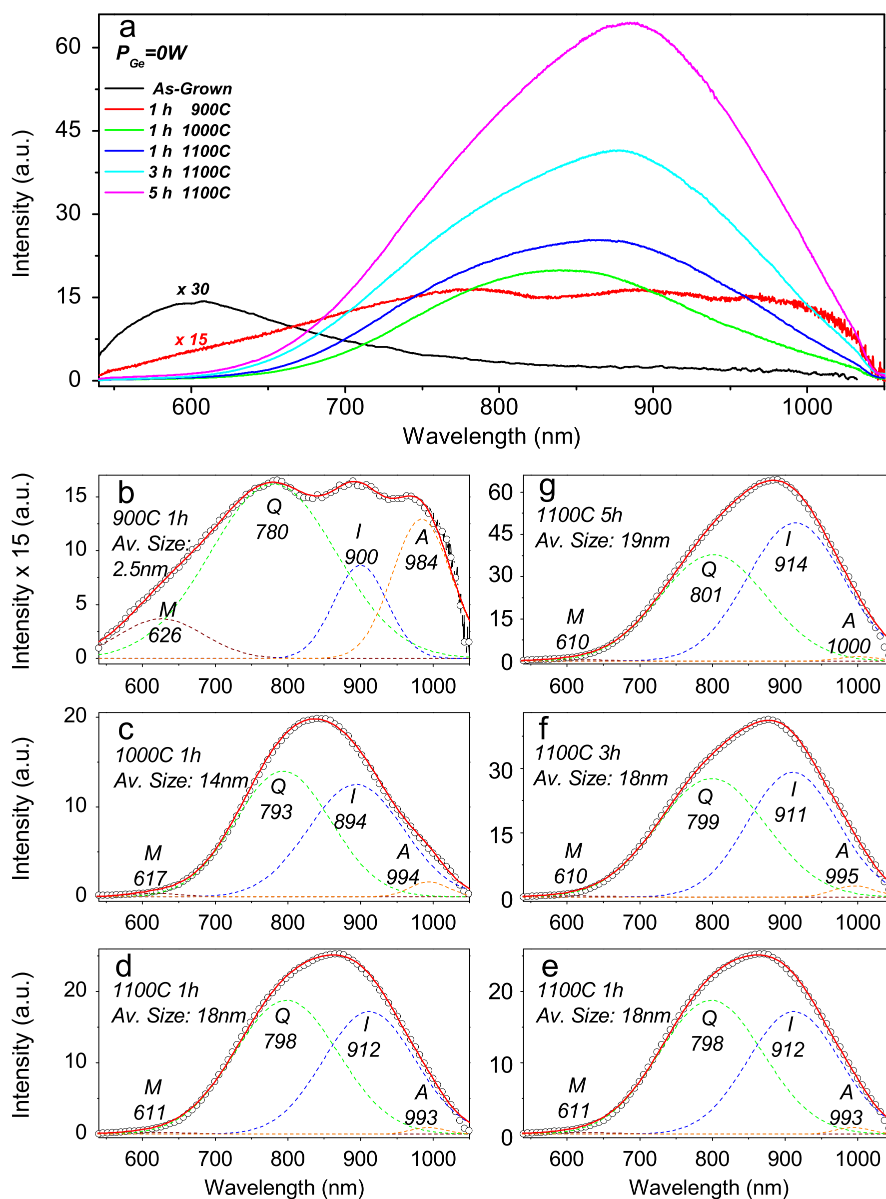

Fig. 4. PL spectra showing (a) the effect of annealing conditions on the SiO_2/Si:Ge:SiO_2/SiO_2 thin films that has no Ge content (P_{Ge}=0 W). PL spectra showing peak fitting analyses of the SiO_2/Si:Ge:SiO_2/SiO_2 thin films that are annealed (b) at T=900 °C for t=1 h, (c) at T=1000 °C for t=1 h, (d and e) at T=1100 °C for t=1 h, (f) at T=1100 °C for t=3 h, and (g) at T=1100 °C for t=5 h.

shown that the as-deposited sample has many kinds of point defects, including neutral oxygen vacancies (NOV) and non-bridging oxygen hole centers (NBOHC), which act as radiative recombination centers or so-called luminescence centers (LCs). The 880 cm^{-1} absorption mode has also been discussed in earlier reports as it is related to the NBOHC situated on Si_6 rings that is located between 570nm and 630 nm and disappears after the post-annealing treatment above 900 °C [35–37]. In this study, the matrix stoichiometry is further improved and the 880 cm^{-1} absorption mode is annealed out by increasing the post-annealing temperature. As a result, we have attributed the signal located at 580 nm for as-grown sample to the matrix related NBOHC centers.

Fig. 6b shows the effect of annealing conditions on the FTIR spectra of both SiO_2/Si:Ge:SiO_2/SiO_2 thin films that were prepared at P_{Ge}=10 W and thermally-grown SiO_2. Post-annealing treatment improves the matrix stoichiometry. The AS mode shifts towards higher frequencies, approaching those of thermally grown SiO_2 films. The type and density of the point defects are expected to change with post-annealing treatment. In the case of a Ge-rich oxide, Si atoms might be substituted by Ge atoms, leading to the formation of two possible modifications such as ≡Si–Ge≡ and ≡Ge–Ge≡ for the neutral oxygen vacancy (NOV) and to the two-fold-coordinated Ge atom. Also, the existence of a divacancy consisting of three neighboring atoms of Si or Ge is assumed [38]. Luminescence between 560 nm and630 nm in Si-rich or Ge-rich SiO_2 was previously reported and several LCs were identified [27,36,39]. Further, the appearance of the low-frequency side shoulder in the FTIR spectra, which covers the Si–O–Ge (~990 cm^{-1}) and Ge–O–Ge (~890 cm^{-1}) vibrations, is attributed to the formation of sub-stoichiometric Ge oxide (GeO_x) during annealing treatment [40]. It appears that the intensity of this shoulder changes with annealing conditions (temperature and time). For prolonged annealing times (3 and 5 h) at 1100 °C, the intensity of Si–O–Si AS mode is decreased, accompanied by an increase in the intensity of the low-frequency side shoulder, implying that additional Si–O–Ge and Ge–O–Ge bonds are formed (Fig. 6a). This feature, together with the evolution of peak M in

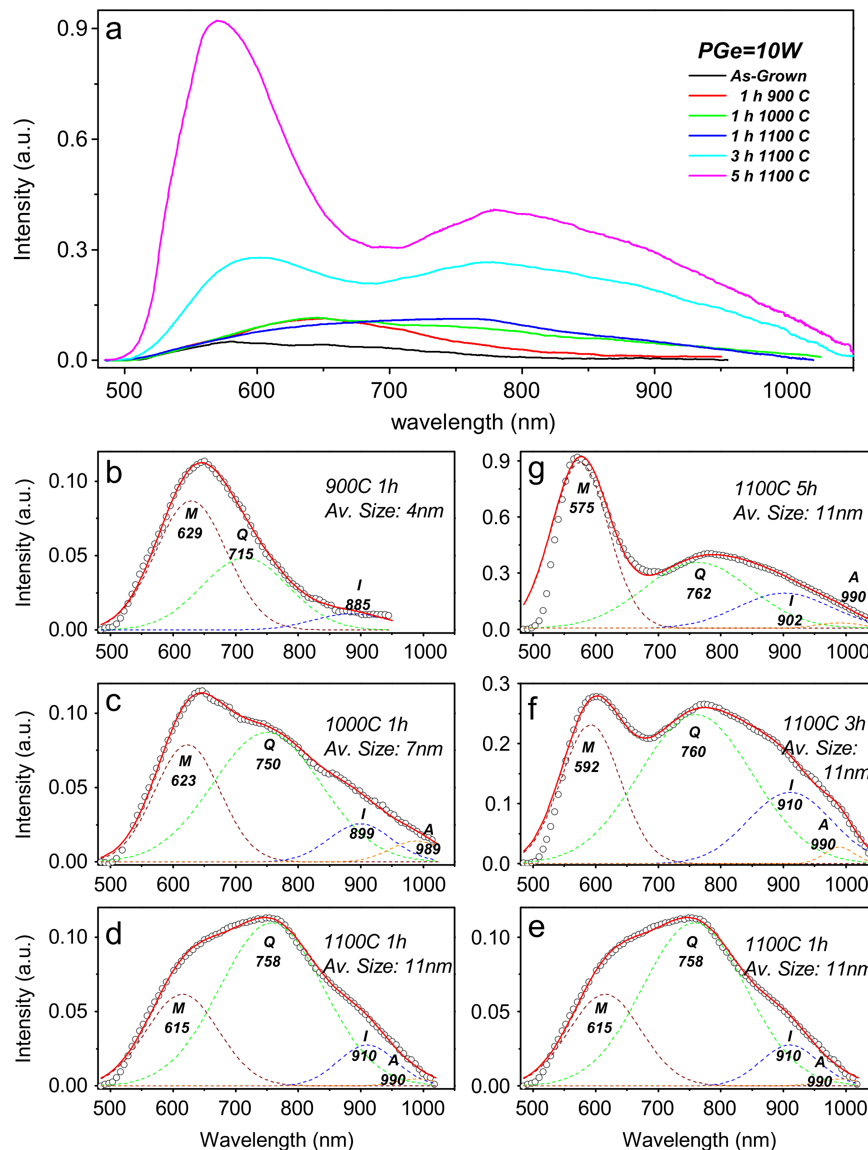

Fig. 5. PL spectra showing (a) the effect of annealing conditions on the SiO_2/Si:Ge:SiO_2/SiO_2 thin films that are prepared using $P_{Ge}=10$ W. PL spectra showing peak fitting analyses of the SiO_2/Si:Ge:SiO_2/SiO_2 thin films that are annealed (b) at $T=900$ °C for $t=1$ h, (c) at $T=1000$ °C for $t=1$ h, (d and e) at $T=1100$ °C for $t=1$ h, (f) at $T=1100$ °C for $t=3$ h, and (g) at $T=1100$ °C for $t=5$ h.

Fig. 5, leads us to attribute peak M to the Ge-related radiative defects located at the sub-oxide (GeO_x), either inside the matrix or at the interface region, which is consistent with the findings of Kartopu et al. [27].

As confirmed also by TEM and XRD analyses, the average sizes of the nanocrystals are 4, 7, and 11 nm for the samples annealed at 900, 1000 to 1100 °C, respectively. The first stages of the phase separation between SiGe and SiO_2 matrix starts at 900 °C, where the SiGe clusters begin to form within the amorphous SiO_2 matrix. There is no well-defined interface between the nanoclusters and the matrix. This means that, for the sample annealed at 900 °C for 1 h (Fig. 5b) the contribution of radiative recombination centers at the sub-oxide (GeO_x), either inside the matrix or at the interface region (peak M, between 570 nm and 629 nm) to the PL spectra is the highest. When the annealing temperature is increased up to 1000 and 1100 °C, crystallization of the SiGe improves (the mean crystal sizes become 7 and 11 nm, respectively) and a well-defined interface between the nanocrystals and the matrix develops. This is accompanied by shift of the peak Q from 715 to 750 nm due to increasing average nanocrystal size (Fig. 5(b–d)). It can also be seen that the peak position is essentially unchanged with prolonged annealing times at 1100 °C, but its intensity increases by about three times. As shown in Ref. [22], the number of large nanocrystals is increased with longer annealing times, whereas the average nanocrystal size does not change appreciably (~11 nm). Thus, it can be concluded that the prolonged annealing can eliminate the nonradiative centers and increase PL peak intensity without increasing the average nanocrystal size.

The most interesting feature of the PL spectra shown in Figs. 4 and 5 is that the signal related to the quantum confinement is located at lower frequencies for Ge-containing samples compared to nc-Si. Although little is known about the effect of crystal size to the nc-Ge electronic structure, various calculations point out that nc-Ge has strong confinement, thus the bandgap of nc-Ge is larger compared to that of nc-Si [2–4,29,41–43]. In an X-ray absorption spectroscopy (XAS) study, on the electronic properties of nc-Ge, Bostedt et al. [43] showed that the quantum size effects for nc-Ge are always stronger than for nc-Si of similar size. More recently, Pan et al. [3] studied the correlation between the size-enlarged Stokes shift and bandgap expansion for nc-Si and nc-Ge

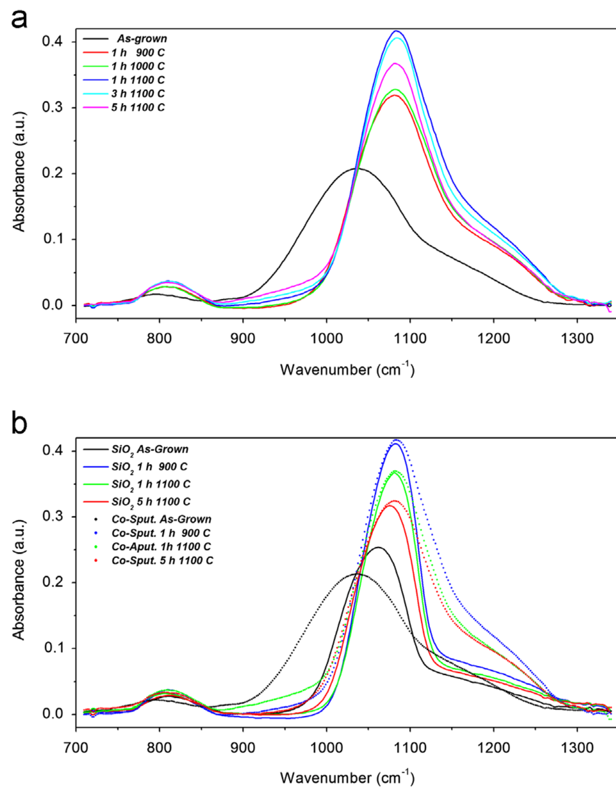

Fig. 6. FTIR spectra showing (a) the effect of annealing conditions on the SiO_2/Si:Ge:SiO_2/SiO_2 thin films that are prepared using $P_{Ge}=10$ W and (b) the comparison of identical annealing conditions on co-sputtered SiO_2/Si:Ge:SiO_2/SiO_2 thin films using P_{Ge}=10 W and only SiO_2 sputtered films.

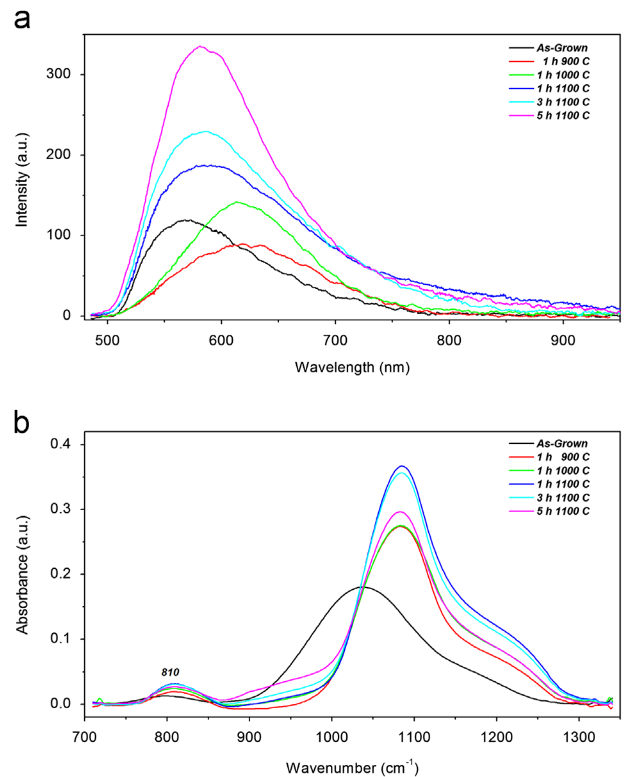

Fig. 7. (a) PL spectra showing the effect of annealing conditions on the SiO_2/Si:Ge:SiO_2/SiO_2 thin films that are prepared using $P_{Ge}=20$ W, and (b) FTIR spectra showing the effect of annealing conditions on the SiO_2/Si:Ge:SiO_2/SiO_2 thin films that are prepared using $P_{Ge}=20$ W.

in terms of bond-order–length–strength correlation. They found out that the bond order deficiency of surface atoms dictates electron–phonon coupling and crystal binding, further, it enhances the size dependence of the observed blueshift in nc-Si and nc-Ge photoemission and photoabsorption spectra. Compared to nc-Si, nc-Ge exhibits stronger electron–phonon coupling due to larger phonon-induced deformation of the crystal lattice. There is an on-going and vibrant discussion on the quantum confinement in nc-Ge. Our experimental results indicate that quantum confinement effects are stronger in nc-$Si_{1-x}Ge_x$ compared to those in pure nc-Si, which is in agreement with previous theoretical reports [4,42].

Compared to Fig. 4 (PL spectra for $P_{Ge}=0$ W), Fig. 5 (PL spectra for $P_{Ge}=10$ W) shows a decrease in relative contribution of the interface-related signal (peak I). This feature is more pronounced in Fig. 7 for the samples prepared with higher applied DC power to Ge ($P_{Ge}=20$ W). In our previous study [28] on the PL properties of nc-Si in the weak quantum confined regime, we have proposed that some of the small nanocrystals contribute to the PL emission according to the model of radiative recombination of the excitons in quantum confinement (peak Q), whereas the others take part in energy transfer into the larger nanocrystals, where radiative recombination through the interface occurs (peak I). In that study, we have also discussed the origin of the interface-related localized states in particular Si=O double bonds at the nc-Si/SiO_2 interface (peak I) in light of room-temperature PL, temperature-dependent PL, and FTIR analyses. Here, in this study, for the samples containing Ge, we mainly attribute the reduced relative contribution of the interface-related component to the appearance of more nonradiative defects especially Ge P_b centers in the nc-$Si_{1-x}Ge_x$/SiO_2 interface [31,32].

Another important factor is that the existence of the silanone structure (Si=O), which is the most stable chemical bond in pure, partially oxidized Si, becomes far less stable in the case of oxidized SiGe. Recently, Dkhissi et al. [44] performed density functional theory calculations on partially oxidized pure Si and SiGe systems by incorporating one, two, and three oxygen atoms to various positions. They demonstrate that Ge atoms hinder O incorporation in their vicinity and in the presence of Ge, the preferential oxidation sites becomes the backbonds of Si atoms, forming dimer units with Ge. In this study for Ge containing samples, we have observed a reduction in the relative contribution of the interface-related luminescence (peak I) and an enhancement in that of the radiative defects-related component (peak M). This observation, accompanied by the decreased intensity of the main AS mode of Si–O–Si vibration and that of high-frequency side shoulder observed in FTIR spectra, and the appearance of a low-frequency side shoulder at 990 cm^{-1} is related to the formation of GeO_x sub-oxide either inside the matrix or at the interface region, especially for the samples with prolonged annealing treatment. The high-frequency side shoulder corresponds to the AS mode of the Si–O–Si bridging bond when two adjacent oxygen atoms move out of phase and is attributed to coupled modes induced by disorder. Additionally, its intensity provides an estimation of the disorder [34]. In the following section, we are going to show PL and FTIR spectra of the samples prepared by $P_{Ge}=20$ W for which the abovementioned features are more pronounced.

The evolution of the peak I for different annealing conditions (duration and temperature) in the samples containing Ge is similar to that of pure nc-Si. Increasing the annealing temperature from 900 to 1100 °C leads to the increase in average nanocrystals size from 3 to 11 nm. Although for the sample annealed at 900 °C, nanocluster agglomeration takes place without a well-defined interface between nanocrystals and the matrix, further increase in the annealing temperature up to 1000 and 1100 °C leads to a formation of larger nanocrystals with a well-defined interface. We attribute the observed redshift in peak I upon increase of the annealing temperature to the increased number of

interface-related radiative defects, which, in turn, leads to the formation of deeper-lying states for larger nanocrystals. Increased intensity of the peak I can be explained by the increased density of the nanocrystals, when annealing temperature is increased up to 1100 °C, hence the increased probability of the energy transfer from small nanocrystals to the larger ones. On the other hand, with a prolonged annealing time at 1100 °C, the average nanocrystal size does not change (~11 nm) but, as discussed above, the size distribution of the nanocrystals evolves from Gaussian-like to log-normal-like in shape. This effect can be the reason for further enhanced intensity of peak I due to increased level of energy transfer between the nanocrystals.

3.2.3. Influence of annealing conditions on nc-$Si_{1-x}Ge_x$ (P_{Ge}=20 W) PL emission

Fig. 7a shows the evolution of the PL spectra with respect to the annealing conditions of the nc-$Si_{1-x}Ge_x$ prepared using P_{Ge}=20 W. The dominant feature of the PL spectra is the peak related to the luminescence from Ge-related radiative defects located at the suboxide (GeO_x), either inside the matrix or at the interface region. For Ge-rich SiO_2 case, Si atoms are most probably substituted by the Ge atoms, which leads to a reduction in the intensity of the main AS mode of Si–O–Si vibrations and strengthening of the low-frequency side shoulder in FTIR spectra (Fig. 7b), which covers the Si–O–Ge (~990 cm^{-1}) and Ge–O–Ge (~890 cm^{-1}) vibrations (GeO_x-related radiative defects). This phenomenon is accompanied by an increased intensity of the defect-related component (peak M) in the PL spectra, where nanocrystal-related components (quantum confinement-related, peak Q, and nc-$Si_{1-x}Ge_x$ interface-related localized states, peak I) have small contributions. We attribute this to the increasing density of Ge P_b centers as Ge content in nc-$Si_{1-x}Ge_x$ is increased. These centers form defect levels in the bandgap and act as the nonradiative recombination centers. As discussed above, our experimental findings of quantum confinement effects are stronger in Ge. Thus, the conclusion of Ge bandgap becoming larger than that of Si is in agreement with theoretical expectations [4,42]. It is worth noting that the localized states in the amorphous Si and/or $Si_{1-x}Ge_x$ bandgap, which contributed considerably to the PL spectra of the samples with no Ge content (P_{Ge}=0 W), especially for the samples that are annealed at lower temperatures (900 °C), have little contribution to the PL spectra of the samples containing higher Ge content (prepared with P_{Ge}=10 and 20 W). This is related to the good miscibility of Si and Ge, which leads to the formation of the SiGe alloy system and also to the decreased crystallization temperature of the $Si_{1-x}Ge_x$ structure as a result of increasing Ge content.

3.2.4. Influence of Ge content on nc-$Si_{1-x}Ge_x$ PL emission under the same annealing conditions

Fig. 8 shows the PL spectra of the samples prepared with different Ge content (P_{Ge}=0, 7, 10, and 20 W) but subjected to the

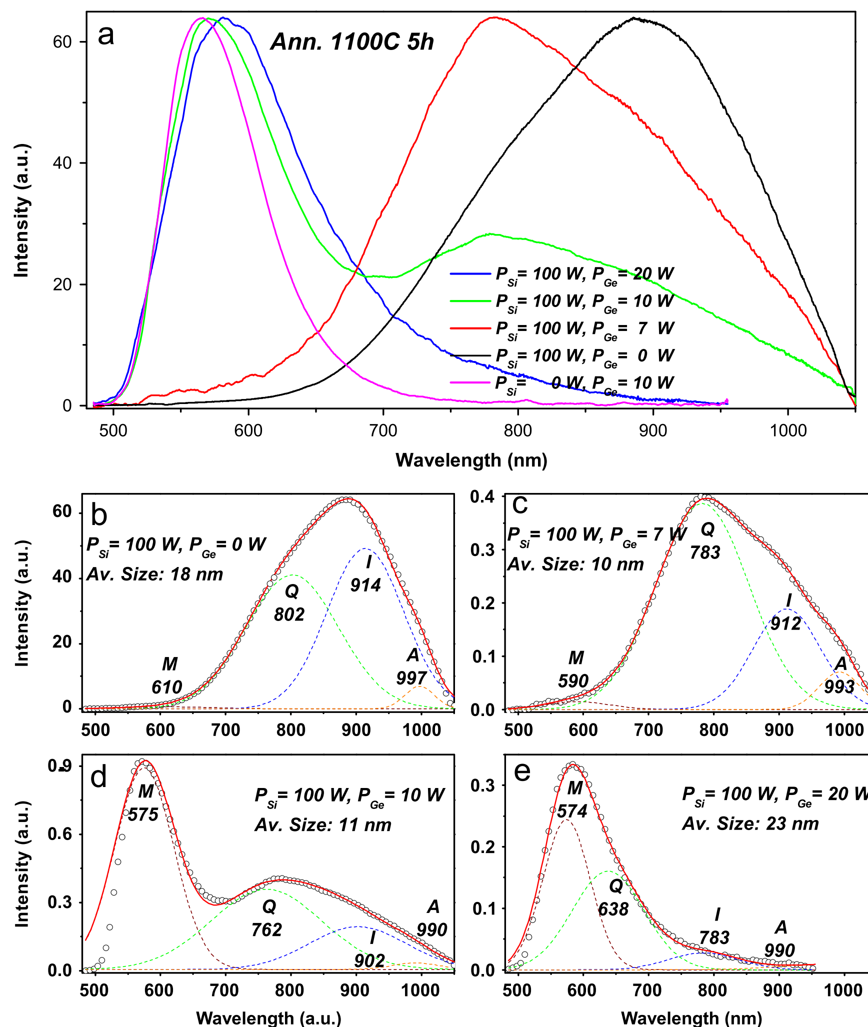

Fig. 8. PL spectra showing (a) the effect of Ge content on the SiO_2/Si:Ge:SiO_2/SiO_2 thin films that are post-annealed at T=1100 °C for t=5 h. PL spectra showing peak fitting analyses of the SiO_2/Si:Ge:SiO_2/SiO_2 thin films that are prepared using (b) P_{Si}=100 W, P_{Ge}=0 W, (c) P_{Si}=100 W, P_{Ge}=7 W, (d) P_{Si}=100 W, P_{Ge}=10 W, and (e) P_{Si}=100 W, P_{Ge}=20 W.

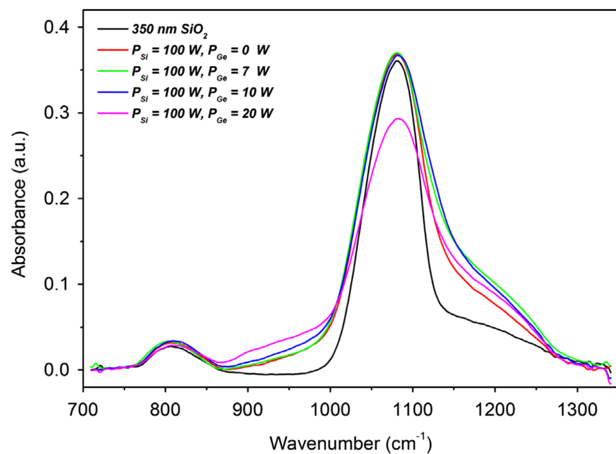

Fig. 9. FTIR spectra showing the effect of Ge content on the $SiO_2/Si:Ge:SiO_2/SiO_2$ thin films that are post-annealed at $T = 1100$ °C for $t = 5$ h.

same annealing treatment (annealed at 1100 °C for 5 h). It also shows the PL spectra of pure nc-Ge, which was annealed at 900 °C for 3 h. It is clearly seen that the spectra blueshifts with increasing Ge content, from a pure nc-Si signal to a pure nc-Ge signal. We also note that the strongest PL signal is obtained from pure nc-Si, which is diminished by about two orders of magnitude with the incorporation of Ge atoms. As discussed above, the reduction of PL intensity with the incorporation of Ge is mainly related to the increased density of Ge P_b centers, which act as nonradiative recombination centers.

In order to clarify the role of Ge content in PL emission, the signal is decomposed into four Gaussian peaks (Fig. 8(b–e)). First, quantum confinement-related signal (peak Q) and the signal assigned to the localized states on the nc-SiO_2 interface (peak I) are dominant for pure nc-Si and for the samples with lower Ge content ($P_{Ge} = 7$ W with $x = 0.42$), whereas for pure nc-Ge and for the samples with higher Ge content ($P_{Ge} = 10$ and 20 W with $x = 0.46$ and 0.70), the Ge-related radiative defects (peak M) play a crucial role. The evolution of the decomposed PL spectra with Ge content is accompanied by the strengthening of the low-frequency side shoulder in the FTIR spectra (Fig. 9), which comprises both Si–O–Ge (~990 cm^{-1}) and Ge–O–Ge (~890 cm^{-1}) vibrations. In addition, a significant reduction in the intensity of main AS mode of Si–O–Si vibrations is observed for the samples prepared using $P_{Ge} = 20$ W. Combining these two observations, it is logical to conclude that peak M can be attributed to the Ge-related radiative defects located at the sub-oxide (GeO_x), either inside the matrix or at the interface region in which Si atoms in Si–O–Si bonds is substituted by the Ge atoms. Apart from that, the most striking observation is the significant spectral blueshift of the quantum confinement-related luminescence (peak Q) with increasing Ge content. This is clear experimental proof that the quantum confinement effects are stronger in Ge, thus the Ge bandgap becomes larger than that of Si. The evaluation of Fig. 8 in light of FTIR spectra (Fig. 9) supports the contribution of peak M to the Ge-related radiative defects located at the sub-oxide (GeO_x), either inside the matrix or at the interface region.

Finally, it is important to discuss the roles of smaller and larger nanocrystals in the PL mechanism. In order to drive clear conclusions, one has to consider the effect of different crystal sizes on the PL emission, from the strong to the weak quantum confinement regime. Takeoka et al. [16] have studied the PL emission of nc-$Si_{1-x}Ge_x$ alloys and observed a near-infrared PL for nanocrystal sizes as small as ~5 nm and with a Ge content of "x" between 0 and 0.31 ($0 < x < 0.31$). They have concluded that the nc-$Si_{1-x}Ge_x$ alloy bandgap energy is similar to that of bulk $Si_{1-x}Ge_x$ alloy crystals and suggested that the PL emission arises from the radiative recombination of excitons confined in SiGe nanocrystals. On the other hand, we have varied the Ge content "x" over a broader range ($0 < x < 1$) and annealing conditions to obtain a wide range of nanocrystal sizes (between 3 nm and 23 nm). Therefore, we are able to identify possible PL mechanisms other than quantum confinement of excitons. These mechanisms include Ge-related radiative defects and nanocrystal-SiO_2 interface-related localized states. Therefore, it is necessary to discuss the origins of nc-$Si_{1-x}Ge_x$ PL emission in consideration of a wide range of nanocrystal sizes.

4. Conclusions

The origins of the PL emission (1.24–2.22 eV) is investigated for nc-Si, nc-Ge, and nc-$Si_{1-x}Ge_x$ embedded in a SiO_2 matrix. We have identified four major luminescence mechanisms: (i) Ge-related radiative defects located at the sub-oxide (GeO_x), either inside the matrix or at the interface region, (ii) nc-$Si_{1-x}Ge_x/SiO_2$ interface-related localized states, (iii) localized states in the amorphous $Si_{1-x}Ge_x$ bandgap and (iv) quantum confinement of excitons in small nanocrystals. It is also found that the nanocrystal size, crystallinity, energy transfer between the nanocrystals, and Ge content are all important factors affecting the PL emission. A gradual blueshift of the PL spectra from the pure nc-Si region to pure nc-Ge region is demonstrated and a clear observation of quantum confinement effect in nc-Ge is presented experimentally. It is also experimentally demonstrated that nc-Ge has a stronger quantum confinement than nc-Si. Furthermore, the decrease in PL intensity with the introduction of Ge to the system is scrutinized. We argue that this decrease can mainly be attributed to the increased density of Ge P_b centers, which act as nonradiative recombination centers. Finally, we distinguish between the roles of smaller and larger nanocrystals in the PL mechanism by changing the mean nanocrystal size from 3 nm to 23 nm (corresponding to a span of the strong to the weak quantum confined regimes).

Acknowledgments

The authors acknowledge the Turkish Ministry of Education (KHK-649/61 md) and TÜBİTAK (The Scientific & Technological Research Council of Turkey) Project Contract no. 106M549 for financial support. The authors also acknowledge the efforts of S. Foss and I. Yildiz in the early stages of this study.

References

[1] S. Takeoka, M. Fuji, S. Hayashi, K. Yamamoto, Phys. Rev. B 58 (1998) 7921.
[2] Y. Maeda, N. Tsukamoto, Y. Yazawa, Y. Kanemitsu, Y. Masumoto, Appl. Phys. Lett. 59 (1991) 3168.
[3] L. Pan, Z. Sun, C. Sun, Scr. Mater. 60 (2009) 1105.
[4] Y.M. Niquet, G. Allan, C. Delerue, M. Lannoo, Appl. Phys. Lett. 77 (2000) 1182.
[5] Y. Maeda, Phys. Rev. B 51 (1995) 1658.
[6] G.S. Armatas, M.G. Kanatzidis, Nano Lett. 10 (2010) 3330.
[7] D.A. Ruddy, J.C. Johnson, E.R. Smith, N.R. Neale, ACS Nano 4 (2010) 7459.
[8] M.V. Wolkin, J. Jorne, P.M. Fauchet, G. Allan, C. Delerue, Phys. Rev. Lett. 82 (1999) 197.
[9] G.G. Qin, Y.J. Li, Phys. Rev. B 68 (2003) 85309.
[10] X.X. Wang, J.G. Zhang, L. Ding, B.W. Cheng, W.K. Ge, J.Z. Yu, Q.M. Wang, Phys. Rev. B 72 (2005) 195313.
[11] A. Saar, Y. Reichman, M. Dovrat, D. Krapf, J. Jedrzejewski, I. Balberg, Nano Lett. 5 (2005) 2443.
[12] J. Martin, F. Cichos, F. Huisken, C.V. Borczyskowski, Nano Lett. 8 (2008) 656.
[13] V.A. Belyakov, V.A. Burdov, R. Lockwood, A. Meldrum, Adv. Opt. Technol. (2008) 279502.
[14] A. Saar, J. Nanophotonics 3 (2009) 032501.
[15] L. Canham, Properties of Porous Silicon, Inspect, London, 1997.
[16] S. Takeoka, K. Toshikiyo, M. Fujii, S. Hayashi, K. Yamamoto, Phys. Rev. B 61 (2000) 15988.

[17] M. Zacharias, R. Weigand, B. Dietrich, F. Stolze, J. Blasing, P. Veit, T. Drusedau, J. Christen, J. Appl. Phys. 81 (1997) 2384.
[18] A. Giorgioni, E. Gatti, E. Grilli, A. Chernikov, S. Chatterjee, D. Chrastina, G. Isella, M. Guzzi, J. Appl. Phys. 111 (2012) 013501.
[19] P. Klenovsky, M. Brehm, V. Krapek, E. Lausecker, D. Munzar, F. Hackl, H. Steiner, T. Fromherz, G. Bauer, J. Humlicek, Phys. Rev. B 86 (2012) 115305.
[20] E.M.F. Vieira, J. Martin-Sanchez, A.G. Rolo, A. Parisini, M. Buljan, I. Capan, E. Alves, N.P. Barradas, O. Conde, S. Bernstorff, A. Chahboun, S. Levichev, M.J.M. Gomes, J. Appl. Phys. 111 (2012) 104323.
[21] S. Ossicini, M. Amato, R. Guerra, M. Palummo, O. Pulci, Nanoscale Res. Lett. 5 (2010) 1637–1649.
[22] N.A.P. Mogaddam, A.S. Alagoz, S. Yerci, R. Turan, S. Foss, T.G. Finstad, J. Appl. Phys. 104 (2008) 124309.
[23] J.P. Dismukes, L. Ekstrom, R.J. Paff, J. Phys. Chem. 68 (1964) 3021.
[24] M.I. Alonso, K. Winer, Phys. Rev. B 39 (1989) 10056.
[25] K. Das, M.L.N. Goswami, A. Dhar, B.K. Mathur, S.K. Ray, Nanotechnology 18 (2007) 175301.
[26] T.V. Torchynska, A. Vivas Hernandez, Y. Goldstein, J. Jedrzejewskii, S. Jimenez-Sandoval, J. Non-Cryst. Solids 352 (2006) 1152.
[27] G. Kartopu, S.C. Bayliss, R.E. Hummel, Y. Ekinci, J. Appl. Phys. 95 (2004) 3466.
[28] N.A.P. Mogaddam, A. Seyhan, A.G. Imer, R. Turan, Photoluminescence from Si nanocrystals embedded in SiO_2 matrix, J. Lumin. (submitted for publication).
[29] G. Kartopu, A.V. Sapelkin, V.A. Karavanskii, U. Serincan, R. Turan, J. Appl. Phys. 103 (2008) 113518.
[30] B. Zhou, S. Pan, S. Chen, C. Li, H. Lai, J. Yu, X. Zhu, J. Lumin. 129 (2009) 1073.
[31] M. Schoisswohl, J.L. Cantin, M. Chamarro, H.J. von Bardeleben, T. Morgenstern, E. Bugiel, W. Kissinger, R.C. Andreu, Phys. Rev. B 52 (1995) 11898.
[32] K. Toshikiyo, M. Tokunaga, Shinji T.M. Fujii, S. Hayashi, J. Appl. Phys. 89 (2001) 4917.
[33] C.T. Kirk, Phys. Rev. B 38 (1988) 1255.
[34] A. Gencer Imer, S. Yerci, A.S. Alagoz, M. Kulakci, U. Serincan, T.G. Finstad, R. Turan, J. Nanosci. Nanotechnol. 10 (2010) 525.
[35] Z. Hajnal, P. Deak, T. Kohler, R. Kaschner, T. Frauenheim, Solid State Commun. 108 (1998) 93.
[36] L. Skuja, Solid State Commun. 84 (1992) 613.
[37] B. Averboukh, R. Huber, K.W. Cheah, Y.R. Shen, G.G. Qin, Z.C. Ma, W.H. Zong, J. Appl. Phys. 92 (2002) 3564.
[38] L. Rebohle, J. von Borany, H. Frob, W. Skorupa, Appl. Phys. B 71 (2000) 131.
[39] C. Itoh, T. Suzuki, N. Itoh, Phys. Rev. B 41 (1990) 3794.
[40] A. Kling, J.C. Soares, A.C. Prieto, J. Jimenez, A. Rodriguez, J. Sangrador, T. Rodriguez, Nucl. Instrum. Methods Phys. Res. B 240 (2005) 405.
[41] T. Takagahara, K. Takeda, Phys. Rev. B 46 (1992) 15578.
[42] N.A. Hill, S. Pokrant, A.J. Hill, J. Phys. Chem. B 103 (1999) 3156.
[43] C. Bostedt, T. van Buuren, T.M. Willey, N. Franco, L.J. Terminello, C. Heske, T. Moller, Appl. Phys. Lett. 84 (2004) 4056.
[44] A. Dkhissi, A.K. Upadhyay, A. Hemeryck, A. Esteve, G. Landa, P. Pochet, M. Djafari Rouhani, Appl. Phys. Lett. 94 (2009) 041912.